Journal of Trace Elements in Medicine and Biology 54 (2019) 98–102

Contents lists available at ScienceDirect

Journal of Trace Elements in Medicine and Biology

journal homepage: www.elsevier.com/locate/jtemb

Quantitative imaging of platinum-based antitumor complexes in bone tissue samples using LA-ICP-MS

Barbara Crone[a,1], Lukas Schlatt[a,1], Robin Abraham Nadar[b], Natasja Wilhelmina Maria van Dijk[b], Nicola Margiotta[c], Michael Sperling[a], Sander Leeuwenburgh[b], Uwe Karst[a,*]

[a] University of Münster, Institute of Inorganic and Analytical Chemistry, Corrensstraße 30, 48149, Münster, Germany
[b] Radboud University Medical Center, Department of Regenerative Biomaterials, Philips van Levdenlaan 25, 6525 EX, Nijmengen, Netherlands
[c] Università degli Studi di BariAldo Moro, Dipartimento di Chimica, Via E. Orabona 4, 70125, Bari, Italy

ARTICLE INFO

Keywords:
Platinum
Cytostatics
Bone tissues
Elemental bioimaging
LA-ICP-MS

ABSTRACT

There is a need for effective medication against bone metastases because todays drugs are not able to penetrate the bone and reach the affected areas. To analyze if current or future platinum-containing drugs are able to achieve this, a quantitative imaging method is urgently needed.

In this study, the platinum distribution in thin sections of mice tibia was determined using laser ablation-inductively coupled plasma-mass spectrometry (LA-ICP-MS) in a spatially resolved manner. The hard bone tissue visible in microscopic images and signals found for calcium and phosphorous recorded via LA-ICP-MS and micro X-ray fluorescence spectroscopy (μXRF) correlate well. Furthermore, the platinum concentration was quantified using polymer-based matrix-matched standards. A limit of detection of 6 μg/g and a linearity of almost three decades could be achieved. Concentrations surpassing 300 μg/g could be found in the tibia samples. The method presented herein is a powerful approach for the visualization and quantification of platinum. As such, this method is a valuable tool to unravel the mechanism of delivery and optimize the therapeutic potency of platinum-containing drugs targeting bone diseases like bone metastases.

1. Introduction

Platinum-based drugs have played a major role in the treatment of cancer ever since the serendipitous discovery of the antitumor activity of cisplatin (*cis*-diamminedichloridoplatinum(II)) more than 50 years ago [1]. To exert its cytostatic effects, cisplatin has to enter the cell where the low chloride ion concentrations facilitate exchange of the chloride ligands for water. The resulting cationic aquo-derivatives of cisplatin can bind to the DNA, altering its structure which inhibits replication and transcription and ultimately induces apoptosis [2]. Even though cisplatin shows a great potency against cancer, there are major drawbacks that complicate its clinical use. The high toxicity toward the kidneys linked to the low selectivity of cisplatin to cancer cells has led to a need for safer alternatives without compromising the desired therapeutic effects [3–5]. Subsequent research has led to the discovery of many cytotoxic compounds including the platinum-based anti-cancer drugs carboplatin and oxaliplatin, which are now approved worldwide for the use against certain types of cancer [6]. These drugs show much lower toxicity compared to cisplatin due to the exchange of ligands for leaving groups which are less likely to aquate [7–9]. However, along with the toxicity, the potency is also decreased since the leaving groups lead to lower amounts of active compounds inside the cells which can interact with the DNA. As an example, in order to achieve similar potencies to cisplatin, the dose of carboplatin administered to patients has to be increased. Another method to increase the potency of cytostatic drugs involves enhancement of the selectivity to tumor cells. For cisplatin and other similar drugs, the increased activity and metabolic rate of tumor cells result in a higher uptake of cisplatin compared to healthy cells [10]. Since systemic damage is typically lower with higher selectivity, these types of drugs could increase potency while simultaneously decreasing toxicity.

In order to advance the potency and safety of these types of drugs, a sensitive detection is necessary. Spatially resolved concentrations can be of high importance in this respect. Due to the very low natural background concentration of platinum in biological tissue and the high sensitivity of the ICP-MS for this element, a sensitive detection can be achieved. Zoriy et al. developed the first method for the visualization of platinum-containing drugs after administration in animal tissue in 2007

* Corresponding author.
E-mail address: uk@uni-muenster.de (U. Karst).
[1] These authors contributed equally.

https://doi.org/10.1016/j.jtemb.2019.04.011
Received 27 August 2018; Received in revised form 21 March 2019; Accepted 18 April 2019
0946-672X/

[11]. Further methods have been developed for hair samples or at higher resolutions to examine the platinum distribution in more detail e.g. in single tumor spheroids [12–14]. The investigation of platinum concentrations in various samples and using different quantifications strategies have been reported in previous studies as well [12–16]. However, to the best of our knowledge, there is no method to quantify platinum in a spatially resolved matter in bone samples yet. This information could be of great interest for the evolution of some types of cancer treatments.

Research in recent years has led to the development of effective anti-cancer drugs [17,18]. Nevertheless, the prognosis for patients strongly depends on the specific type of cancer. Especially if metastasis to the bone is observed, the median survival after diagnosis is very short, ranging between a few months and a few years, depending on the tumor type [19]. Furthermore, bone metastases are a major cause for morbidity, characterized by severe pain and bone fractures or spinal cord compressions [20]. Medications like bisphosphonates can help in slowing the tumor growth and aid in reducing the pain, but the cancer can rarely be cured after metastasis [21]. Generally, current treatment options against bone metastases are unsatisfactory and scarce. A plausible explanation for this phenomenon relates to the fact that anti-cancer drugs are not effectively delivered to the bone, where they have to exert their cytostatic effects. To further understand and optimize the distribution of cytostatic drugs in bone, a sensitive and spatially resolved analysis method is urgently required.

In this study, an imaging technique employing laser ablation-inductively coupled plasma-mass spectrometry (LA-ICP-MS) to analyze the uptake of platinum-containing anti-cancer drugs into hard bone tissue is presented. Platinum(II) dinitrate ethylenediamine (*cis*-[Pt$(NO_3)_2$(en)], en = ethylenediamine) was used as a model compound for platinum-based antitumor drugs since it is commonly used as a precursor in the synthesis of similar drugs such as the Pt-bisphosphonate complexes [22]. Matrix-matched standards based on Technovit® were used for platinum quantification by external calibration. Prior to spatially resolved analysis via LA-ICP-MS, micro X-ray fluorescence spectroscopy (μXRF) was used to obtain a first impression of the elemental distribution and to visualize characteristic elements in bone tissue such as phosphorous and calcium.

2. Experimental

2.1. Animals and sample preparation

C57BL/6NCrl mice were treated with 1.25 μmol platinum, which corresponds to 0.5 mg of *cis*-[Pt$(NO_3)_2$(en)] by injecting a saline solution of the substance intravenously via the tail veins of the mice. After removing the tibia samples, bones were incubated in neutral buffered formaldehyde for 36 h. Tibias were dehydrated in ascending grades of 70%–100% ethanol and embedded in poly(methyl methacrylate) (pMMA) resin, freshly prepared by mixing 600 mL of methyl methacrylate monomer (Acros Organics BVBA, Geel, Belgium), 60 ml dibutyl phthalate (Merck KGaA, Darmstadt, Germany) and 1.25 g perkadox®16 (Aldrich, Zwijndrecht, Netherlands). The polymerization was followed by cutting serial horizontal sections (perpendicular to the tibia sample) of 5 μm thickness within the trabecular region of interest using an RM2155 microtome with a TC 65 blade (Leica Microsystems GmbH, Wetzlar, Germany).The workflow for sample preparation is presented in(Fig. 1).

Microscopic images were obtained using an inverted fluorescence/bright field microscope (BZ-9000, Keyence Deutschland GmbH, Neu-Isenburg, Germany). For image recording and processing, the software BZ-II Viewer and BZ-II Analyzer were used, respectively.

2.2. Quantification strategy

The quantification strategy is based on matrix-matched external calibration and the quantitative ablation of thin sections of bone samples and standards. Since both are prepared by using the same embedding medium and the density of the embedded tissue equals the density of the embedding medium, this results in very similar ablation behavior. For this reason, the matrix.matching can be performed by using the embedding medium as a model for the embedded tissue [23]. For external calibration, eight matrix-matched standards based on Technovit 7100® (a polymer based on 2-hydroxyethylmethacrylate (HEMA)) were prepared, ranging from 0 to 1000 μg/g platinum. Preparation and characterization of the standards were performed as described by Reifschneider et al. [23] The infiltration solution was spiked with platinum(II) acetylacetonate and diluted to obtain different platinum concentrations. After polymerization, sections of 5 μm thickness were prepared using a rotary microtome (HM 355S, Thermo Scientific, Waltham, MA) and mounted onto microscopic slides.

The limit of detection and limit of quantification were determined by the 3σ and 10σ criteria to be 6 μg/g and 20 μg/g respectively. A linear correlation could be observed up to a concentration of 1000 μg/g with a correlation coefficient (R^2) of 0.9997. The calibration was performed on three separate days to validate the calibration data and examine the reproducibility of the method. The correlation coefficient (R^2) was always greater than 0.995 and the slope of the calibration curve only showed a variation of 8% between measurements.

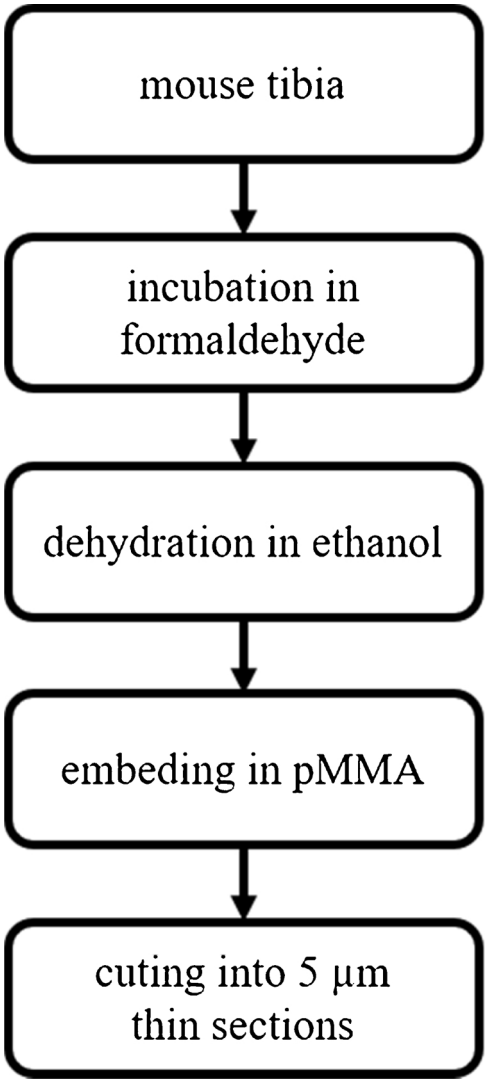

Fig. 1. Scheme for the preparation of mouse tibia samples prior to analysis.

2.3. μXRF analysis

The bone samples were examined by non-destructive μXRF using a TORNADO M4 X-ray spectrometer (Bruker Nano, Berlin, Germany). The system was equipped with an X-ray tube using rhodium as anode material and a polycapillary optics to focus the incident X-ray beam. The X-ray tube was set to an anode voltage of 50 kV and anode current of 600 μA. Analyses were performed under vacuum (20 mbar) to avoid interferences and signal overlaps with argon and other elements present in ambient air. The samples were placed on the mobile stage and mapped with a spot size of 25 μm and a spacing of 10 μm between each spot. The acquisition time was set to 10 ms per spot. The emitted X-ray fluorescence of the Ca-K_α line (3.691 keV), Pt-L_α line (9.435 keV), P-K_α line (2.010 keV) and S-K_α line (2.309 keV) were detected by a silicon drift detector (SDD, XFlash® 5030, Bruker Nano GmbH). Signal intensities per pixel from 20 cycles were averaged. Data evaluation and image processing were carried out by the software ESPRIT HyperMap (Bruker GmbH, Germany).

2.4. Imaging by LA-ICP-MS

Elemental analysis by LA-ICP-MS was performed with the commercially available system LSX 213 $G2^+$ (CETAC Technologies, Omaha, USA) using a frequency quintupled Nd:YAG laser at a wavelength of 213 nm. The laser ablation system was coupled to a triple-quadrupole based iCAP TQ ICP-MS (Thermo Fisher Scientific, Bremen, Germany). The laser spot size was set to 10 μm with a scan speed of 20 μm/s and a laser shot frequency of 20 Hz. The samples were completely ablated using a line-by-line mode to facilitate quantification. The aerosol generated by the LA was transported to the ICP-MS system by a gas mixture of 0.8 L/min helium and 1.0 L/min argon (tuned daily), which was added after the ablation cell. The ICP-MS torch was equipped with a quartz injector pipe with an inner diameter of 3.5 mm and the interface consisted of sampler and skimmer cones based on nickel. Platinum, calcium and phosphorous were detected in mass shift mode using the second quadrupole as reaction cell with oxygen as reaction gas (0.43 L/min) and the first and third quadrupole as mass filters. Calcium and phosphorous were measured as $^{40}Ca^{16}O^+$ and $^{31}P^{16}O^+$, platinum was detected on mass as $^{195}Pt^+$. The following ICP-MS parameters were applied: rf power, 1550 W; auxiliary gas flow, 0.80 L/min and cool gas flow, 14 L/min. Ablation profiles were examined and evaluated using in-house developed software.

3. Results and discussion

3.1. Bone analysis by means of μXRF

Non-destructive μXRF measurements were performed in order to obtain a first overview of the bone samples. Fig. 2 shows the elemental distribution of calcium, phosphorous and sulfur in a mouse tibia containing *cis*-[$Pt(NO_3)_2$(en)] (Fig. 2b–d). The sampled bone tissue section is a part of the metaphysis region of the proximal tibia, which is a common site for bone metastasis [24,25].

Along with the light microscopic image of the tibia sample (Fig. 2a), an overlay of the calcium distribution (Fig. 2e) is shown. Calcium (Fig. 2b) can be used to visualize the hard bone structures, which are shown through darker areas in the microscopic image. Here, the optical image and the calcium distribution are in good accordance. A similar distribution pattern was obtained for phosphorous (Fig. 2c), representing the harder bone structures as well. The distribution pattern of sulfur (Fig. 2d) shows slight differences in comparison with the distribution of calcium and phosphorous since sulfur is derived from organic components in bone tissue. The spatial distribution of platinum could not be obtained by μXRF since it was below the detection limit.

Using a bench-top μXRF, the major bone elements calcium and phosphorous in the hard bone tissue as well as sulfur representing organic components in bone could successfully be detected. Previous studies have already focused on the analysis of bone by polycapillary-focused scanning μ-XRF. Voglis et al. performed elemental mapping of human femur with a laboratory-developed microbeam XRF [26]. In addition to elements like aluminum, chlorine, chromium and potassium, the spatial distribution of calcium, phosphorous and sulfur were presented. Different major and minor trace elements in a metal implant as well as hard bone and soft tissue were investigated by Blaske et al. using μXRF and LA-ICP-MS [27]. Platinum was not discussed in these studies but besides the detection of titanium and vanadium as implant metals, μXRF was used to analyze calcium and phosphorous for hard bone tissue and sulfur as marker for soft tissue.

Due to the non-destructive analysis mode of μXRF, further investigations of the same samples can be performed by other techniques. LA-ICP-MS offers a higher sensitivity and spatial resolution as well as the possibility for quantitative analyses. Thus, it is a powerful alternative to quantify platinum in soft and hard tissue samples. Reifschneider et al. demonstrated this in cochlea and surrounding tissue [23].

3.2. Quantitative imaging of mouse tibia by LA-ICP-MS

The spatial distribution of platinum in mouse tibia was investigated by means of LA-ICP-MS after treatment with platinum dinitrate ethylenediamine ([$Pt(NO_3)_2$(en)]). Quantitative platinum analysis was performed using an external calibration based on matrix-matched standards. The distributions of platinum, calcium and phosphorous are depicted in Fig. 3. Calcium and phosphorous were measured in mass shift mode of the TQ-MS as $^{40}Ca^{16}O^+$ and $^{31}P^{16}O^+$. Additionally, the microscopic image (Fig. 3a) and an overlay of the calcium and platinum distribution pattern (Fig. 3e) are shown.

The calcium distribution (Fig. 3b) clearly shows the trabecular bone structure which correlates well with the dark-colored features in the microscopic image (Fig. 3a). The spatial phosphorous distribution (Fig. 3c) shows a similar pattern compared to calcium and can therefore be used to visualize hard bone tissue as well. These results stand in good accordance with those obtained by μXRF. The quantification of platinum (Fig. 3d) reveals local concentrations surpassing 300 μg/g. Highest concentrations were found on the outside of the bone samples, while only minor concentrations (30–100 μg/g Pt) were detected in the center of the bone samples. The overlay of calcium and platinum clearly shows that the high concentrations of platinum (shown in green) on the outside of the bone sample are not co-localized with the hard bone tissue, which is represented by calcium (shown in red). If both elements are detected in the same area, it is represented in yellow as can be seen in minor areas in the center of the image (Fig. 3e). This demonstrates that *cis*-[$Pt(NO_3)_2$(en)] is not able to effectively penetrate into bone. Since the acquisition time necessary for a sample of this size, with a resolution of 10 μm, was about 10 h it was further investigated if a lower resolution of 25 μm would be suitable to demonstrate the lack of platinum penetration into hard bone tissue. Fig. 4 shows a comparison of two bone samples recorded at a spot size of 10 μm (Fig. 4 top) and 25 μm (Fig. 4 bottom). While the lower resolution of the recoded image is noticeable, it can still be seen that the platinum is mostly located in a band around the hard bone tissue. Furthermore, just like in the higher resolution sample, very little co-localization can be observed. Due to the much lower acquisition time of only about 3 h this lower resolution should be chosen for routine analysis. Nonetheless, both 25 μm and 10 μm can be selected based on the requirements of the sample.

To further examine the extent of calcium-platinum co-localization, a numeric estimation of the ability of the drugs to penetrate the hard bone tissue can be determined by calculating the percentage of platinum which is co-localized with calcium. To do so, first the background of the image and therefore all pixels without hard bone tissue have to be discarded from the calculations. In this case, a pixel is considered to be background if its calcium intensity is of the lowest 15%. The platinum

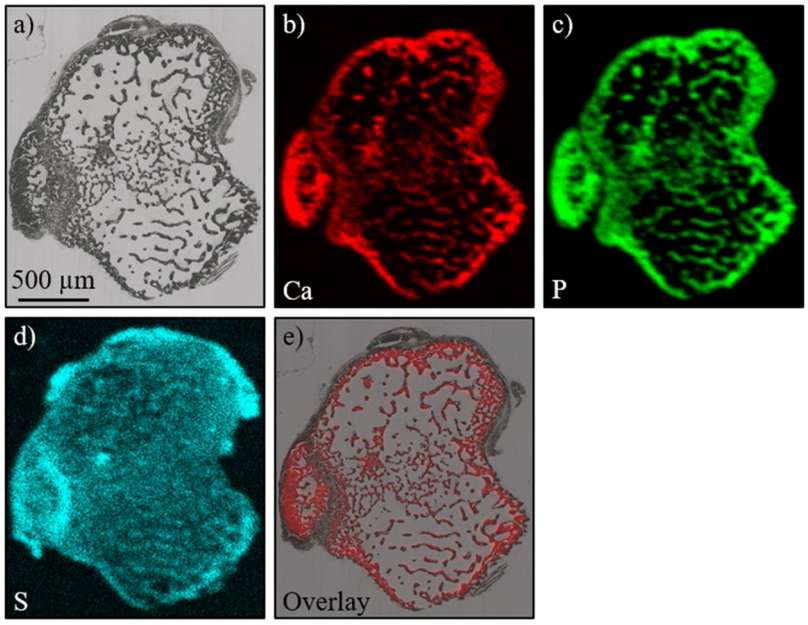

Fig. 2. Mouse tibia investigated by µXRF. The microscopic image of the sample exposed to $[Pt(NO_3)_2(en)]$ (a) is shown along with the distribution patterns of calcium (b), phosphorous (c) and sulfur (d). An overlay of the microscopic image with the calcium distribution (e) is also presented.

concentrations of the remaining pixels are then added up and divided by the sum of the entire platinum image to yield the percentage of platinum co-localized with calcium. Such an evaluation of the high-resolution sample shows that only 54.4% of the platinum detected is co-localized with calcium. Taking into account that the tibia thin section consists almost exclusively of hard bone tissue, the amount of co-localized platinum is relatively low.

4. Conclusion

In this study, a quantitative method for mass spectrometric imaging was developed to investigate the distribution of platinum in mouse tibia after administration of *cis*-$[Pt(NO_3)_2(en)]$ as model for platinum-based antitumor drugs such as cisplatin. First, non-destructive µXRF was used to investigate the calcium, phosphorous and sulfur distribution. Subsequently, LA-ICP-MS analysis was performed to visualize the platinum distribution. Using an external calibration with standards based on the polymer Technovit®, the platinum signal could be quantified and concentrations up to 300 µg/g were found. This distribution could be compared to those of calcium and phosphorous, which were used to represent the inorganic component of bone tissue. Platinum did not effectively penetrate the bone but was found at its highest

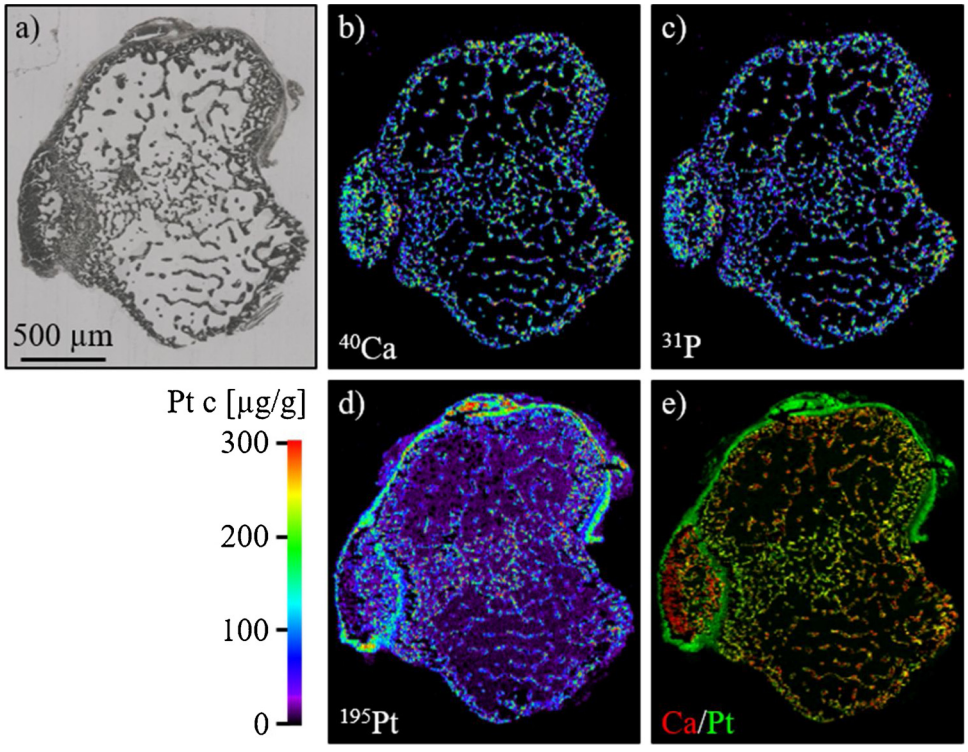

Fig. 3. Quantitative platinum distribution in mouse tibia obtained by LA-ICP-MS. The microscopic image of the investigated sample (a); calcium distribution (b); phosphorous distribution (c); platinum distribution (d) and an overlay calcium (red) and platinum (green) (e) is shown. Co-localization of platinum and calcium is indicated in yellow (For interpretation of the references to colour in this figure legend, the reader is referred to the web version of this article).

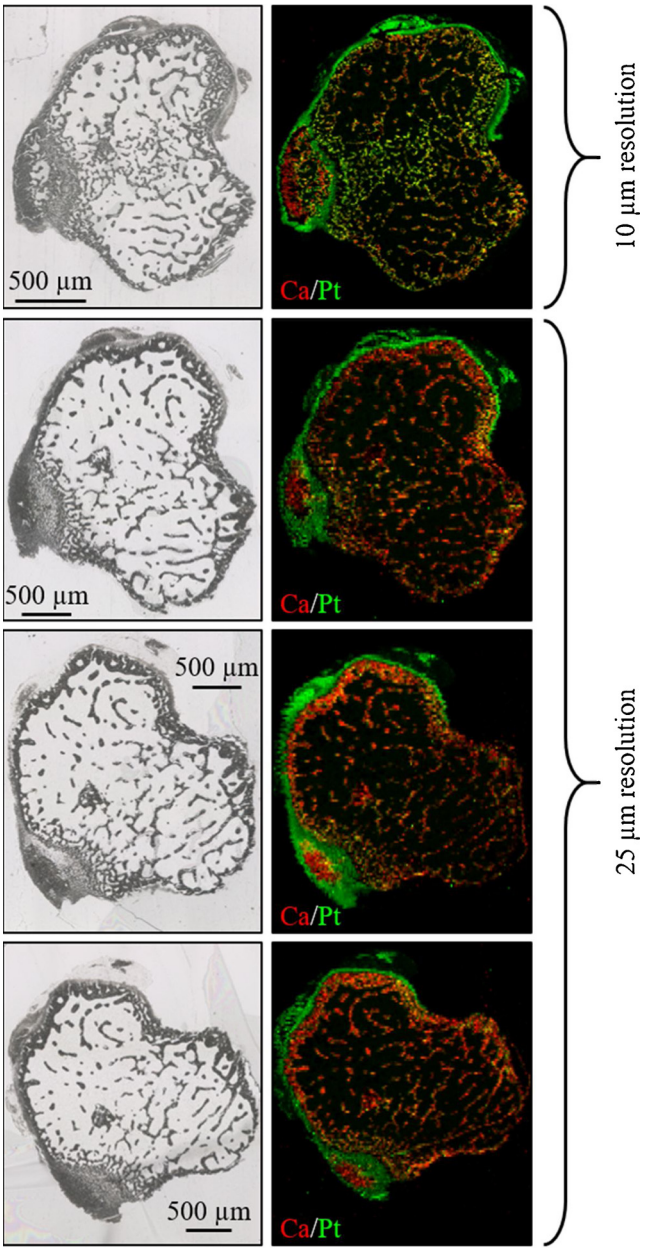

Fig. 4. Microscopic images of mouse tibia samples along with LA-ICP-MS overlays of the calcium (red) and platinum (green) distributions. The sample shown on top was recorded at a resolution of 10 µm while the other samples have a lower resolution of 25 µm (For interpretation of the references to colour in this figure legend, the reader is referred to the web version of this article).

concentrations outside the bone. In order to be effective against bone metastasis, cytostatic drugs should be able to penetrate into bone. Using this method, the bone-penetrating properties of new types of bone-targeted platinum-containing cancer medication can be examined in order to develop effective medication against bone metastases.

Conflict of interest

All authors declare that there are no conflicts of interest associated with this manuscript.

References

[1] B. Rosenberg, L. van Camp, T. Krigas, Inhibition of cell division in Escherichia coli by electrolysis products from a platinum electrode, Nature 205 (1965) 698–699, https://doi.org/10.1038/205698a0.
[2] L. Kelland, The resurgence of platinum-based cancer chemotherapy, Nat. Rev. Cancer 7 (2007) 573–584, https://doi.org/10.1038/nrc2167.
[3] V. Launay-Vacher, J.-B. Rey, C. Isnard-Bagnis, G. Deray, M. Daouphars, Prevention of cisplatin nephrotoxicity: state of the art and recommendations from the European Society of Clinical Pharmacy Special Interest Group on Cancer Care, Cancer Chemother. Pharmacol. 61 (2008) 903–909, https://doi.org/10.1007/s00280-008-0711-0.
[4] N. Pabla, Z. Dong, Cisplatin nephrotoxicity: mechanisms and renoprotective strategies, Kidney Int. 73 (2008) 994–1007, https://doi.org/10.1038/sj.ki.5002786.
[5] R. Skinner, Best practice in assessing ototoxicity in children with cancer, Eur. J. Cancer 40 (2004) 2352–2354, https://doi.org/10.1016/j.ejca.2004.08.002.
[6] A.R. Timerbaev, C.G. Hartinger, S.S. Aleksenko, B.K. Keppler, Interactions of antitumor metallodrugs with serum proteins: advances in characterization using modern analytical methodology, Chem. Rev. 106 (2006) 2224–2248, https://doi.org/10.1021/cr040704h.
[7] K.R. Harrap, Preclinical studies identifying carboplatin as a viable cisplatin alternative, Cancer Treat. Rev. 12 (1985) 21–33, https://doi.org/10.1016/0305-7372(85)90015-5.
[8] N.J. Wheate, S. Walker, G.E. Craig, R. Oun, The status of platinum anticancer drugs in the clinic and in clinical trials, Dalton Trans. 39 (2010) 8113–8127, https://doi.org/10.1039/c0dt00292e.
[9] T. Alcindor, N. Beauger, Oxaliplatin: a review in the era of molecularly targeted therapy, Curr. Oncol. 18 (2011) 18–25, https://doi.org/10.3747/co.v18i1.708.
[10] I. Ott, R. Gust, Medizinische Chemie der Platinkomplexe: Besonderheiten anorganischer Zytostatika, Pharm. Unserer Zeit 35 (2006) 124–133, https://doi.org/10.1002/pauz.200500161.
[11] M. Zoriy, A. Matusch, T. Spruss, J.S. Becker, Laser ablation inductively coupled plasma mass spectrometry for imaging of copper, zinc, and platinum in thin sections of a kidney from a mouse treated with cis-platin, Int. J. Mass Spectrom. 260 (2007) 102–106, https://doi.org/10.1016/j.ijms.2006.09.012.
[12] D. Gholap, J. Verhulst, W. Ceelen, F. Vanhaecke, Use of pneumatic nebulization and laser ablation–inductively coupled plasma–mass spectrometry to study the distribution and bioavailability of an intraperitoneally administered Pt-containing chemotherapeutic drug, Anal. Bioanal. Chem. 402 (2012) 2121–2129, https://doi.org/10.1007/s00216-011-5654-3.
[13] M. Bonta, H. Lohninger, V. Laszlo, B. Hegedus, A. Limbeck, Quantitative LA-ICP-MS imaging of platinum in chemotherapy treated human malignant pleural mesothelioma samples using printed patterns as standard, J. Anal. At. Spectrom. 29 (2014) 2159–2167, https://doi.org/10.1039/C4JA00245H.
[14] C. Köppen, O. Reifschneider, I. Castanheira, M. Sperling, U. Karst, G. Ciarimboli, Quantitative imaging of platinum based on laser ablation-inductively coupled plasma-mass spectrometry to investigate toxic side effects of cisplatin, Metallomics 7 (2015) 1595–1603, https://doi.org/10.1039/C5MT00226E.
[15] O.B. Bauer, C. Köppen, M. Sperling, H. Schurek, G. Ciarimboli, U. Karst, Quantitative bioimaging of platinum via online isotope dilution-laser ablation-inductively coupled plasma mass spectrometry, Anal. Chem. 90 (2018) 7033–7039, https://doi.org/10.1021/acs.analchem.8b01429.
[16] B. Crone, M. Aschner, T. Schwerdtle, U. Karst, J. Bornhorst, Elemental bioimaging of cisplatin in Caenorhabditis elegans by LA-ICP-MS, Metallomics 7 (2015) 1189–1195, https://doi.org/10.1039/C5MT00096C.
[17] E. Wong, C.M. Giandomenico, Current status of platinum-based antitumor drugs, Chem. Rev. 99 (1999) 2451–2466, https://doi.org/10.1021/cr980420v.
[18] M. Galanski, V. Arion, M. Jakupec, B. Keppler, Recent developments in the field of tumor-inhibiting metal complexes, Curr. Pharm. Des. 9 (2003) 2078–2089, https://doi.org/10.2174/1381612033454180.
[19] G. Selvaggi, G.V. Scagliotti, Management of bone metastases in cancer: a review, Crit. Rev. Oncol. Hematol. 56 (2005) 365–378, https://doi.org/10.1016/j.critrevonc.2005.03.011.
[20] M.G. Cecchini, A. Wetterwald, G. van der Pluijm, G.N. Thalmann, Molecular and biological mechanisms of bone metastasis, EAU Update Ser. 3 (2005) 214–226, https://doi.org/10.1016/j.euus.2005.09.006.
[21] F. Macedo, K. Ladeira, F. Pinho, N. Saraiva, N. Bonito, L. Pinto, F. Gonçalves, Bone metastases: an overview, Oncol. Rev. 11 (2017) 321, https://doi.org/10.4081/oncol.2017.321.
[22] M. Iafisco, N. Margiotta, Silica xerogels and hydroxyapatite nanocrystals for the local delivery of platinum–bisphosphonate complexes in the treatment of bone tumors: a mini-review, J. Inorg. Biochem. 117 (2012) 237–247, https://doi.org/10.1016/j.jinorgbio.2012.06.004.
[23] O. Reifschneider, C.A. Wehe, I. Raj, J. Ehmcke, G. Ciarimboli, M. Sperling, U. Karst, Quantitative bioimaging of platinum in polymer embedded mouse organs using laser ablation ICP-MS, Metallomics 5 (2013) 1440–1447, https://doi.org/10.1039/c3mt00147d.
[24] H.K. Brown, P.D. Ottewell, C.A. Evans, I. Holen, Location matters: osteoblast and osteoclast distribution is modified by the presence and proximity to breast cancer cells in vivo, Clin. Exp. Metastasis 29 (2012) 927–938, https://doi.org/10.1007/s10585-012-9481-5.
[25] P.A. Phadke, Kinetics of metastatic breast cancer cell trafficking in bone, Clin. Cancer Res. 12 (2006) 1431–1440, https://doi.org/10.1158/1078-0432.CCR-05-1806.
[26] P. Voglis, A. Attaelmanan, P. Engström, S. Larsson, A. Rindby, K. Boström, C.G. Helander, Elemental mapping of bone tissues by the use of capillary focused XRF, X-Ray Spectrom. 22 (1993) 229–233, https://doi.org/10.1002/xrs.1300220411.
[27] F. Blaske, O. Reifschneider, G. Gosheger, C.A. Wehe, M. Sperling, U. Karst, G. Hauschild, S. Höll, Elemental bioimaging of nanosilver-coated prostheses using X-ray fluorescence spectroscopy and laser ablation-inductively coupled plasma-mass spectrometry, Anal. Chem. 86 (2014) 615–620, https://doi.org/10.1021/ac4028577.